Review in Advance first posted online on November 21, 2013. (Changes may still occur before final publication online and in print.)

Superresolution Localization Methods

Alexander R. Small[1] and Raghuveer Parthasarathy[2]

[1]Department of Physics and Astronomy, California State Polytechnic University, Pomona, California 91768

[2]Department of Physics, The University of Oregon, Eugene, Oregon 97403; email: raghu@uoregon.edu

Annu. Rev. Phys. Chem. 2014. 65:107–25

The *Annual Review of Physical Chemistry* is online at physchem.annualreviews.org

This article's doi: 10.1146/annurev-physchem-040513-103735

Keywords

fluorescence microscopy, image processing, PALM, STORM, photoswitchable molecules, blinking microscopy, maximum likelihood estimation, Cramer-Rao lower bound, point spread function

Abstract

Superresolution localization microscopy methods produce nanoscale images via a combination of intermittently active fluorescent probes and algorithms that can precisely determine the positions of these probes from single-molecule or few-molecule images. These algorithms vary widely in their underlying principles, complexity, and accuracy. In this review, we begin by surveying the principles of localization microscopy and describing the fundamental limits to localization precision. We then examine several different families of fluorophore localization algorithms, comparing their complexity, performance, and range of applicability (e.g., whether they require particular types of experimental information, are optimized for specific situations, or are more general). Whereas our focus is on the localization of single isotropic emitters in two dimensions, we also consider oriented dipoles, three-dimensional localization, and algorithms that can handle overlapping images of several nearby fluorophores. Throughout the review, we try to highlight practical advice for users of fluorophore localization algorithms, as well as open questions.

1. INTRODUCTION

Accurately and precisely determining the positions of individual point-like objects in digital images has long been an important task in many diverse fields. These applications include, for example, finding stars in astronomical images (1), inferring forces between colloidal particles in fluids (2), and characterizing the motions of biomolecules such as molecular motors (3). Recent years have brought the realization that single-molecule localization can also be used to construct images that transcend the diffraction limit of traditional microscopy, allowing unprecedented views of cellular structures at sub-100-nm scales (4–10). Several closely related techniques of localization-based superresolution microscopy have emerged, capturing a great deal of attention among molecular and cell biologists, biophysicists, and others. All these techniques rely on sequentially imaging sparse subsets of the fluorophores labeling a sample (sparse enough that each image consists mainly of well-separated single molecules), precisely measuring the position of each imaged fluorophore, and reconstructing an image from the set of all positions. This can be implemented in a variety of ways, in two or three dimensions.

The accuracy and robustness of particle localization algorithms are crucial to superresolution microscopy. This has spurred a flurry of research into localization methods, and it also raises key practical questions for superresolution practitioners: What are the fundamental bounds on localization precision in digital images? What localization methods exist, and what are their features and flaws? How can we assess the precision and accuracy of localization methods? We address these questions in this review. We first comment on traditional microscopy and discuss the experimental implementation of superresolution techniques, but briefly, as this is described in several other recent reviews (8–10).

2. LOCALIZATION-BASED SUPERRESOLUTION MICROSCOPY

Fluorescence microscopy is a powerful tool for biological investigation, as the labeling of biomolecules with either extrinsic or genetically encoded fluorophores enables identification of specific cellular components involved in various processes. The small size of subcellular machineries—microtubules 25 nm in diameter, transport vesicles approximately 100 nm in size, 30-nm-wide chromatin fibers, to give just a few examples—presents a challenge for fluorescence microscopy, as well as all other approaches that use visible light.

Photons emitted by a point source, when imaged onto any detector by any optical system, are not focused to a point. Rather, because of the diffraction inherent in the wave-like nature of light, the photons are smeared out with a spatially extended probability distribution. This distribution is known as the point spread function (PSF) of the imaging system, and it has a characteristic width $\Delta \approx \lambda/(2\ \mathrm{NA})$, where λ is the wavelength of light and NA is the numerical aperture of the imaging system. The numerical aperture is the product of the index of refraction of the imaging medium and the sine of the maximum angle of collected rays with respect to the optical axis, and it is therefore constrained in practice to be at most NA $\approx$ 1.4. For visible light, λ is of order 500 nm, for example, $\lambda = 508$ nm for the peak emission of green fluorescent protein, so $\Delta \approx$ 200 nm. The intensity distributions of sources spatially separated by less than Δ will overlap considerably, and the sources will therefore not be resolvable as distinct objects (**Figure 1*a*,*b***). Thus we have the well-known diffraction limit of optical microscopy, which sets a strong lower bound on the sizes of structures that can be imaged. Using smaller wavelengths is generally not possible—many biomaterials autofluoresce in the ultraviolet (UV) spectrum, and UV light is readily absorbed by many biomolecules and also causes significant photodamage.

Although the width of the PSF determines the resolvability of adjacent fluorophores, the position of a single fluorophore (i.e., the PSF's center) can be determined with precision much

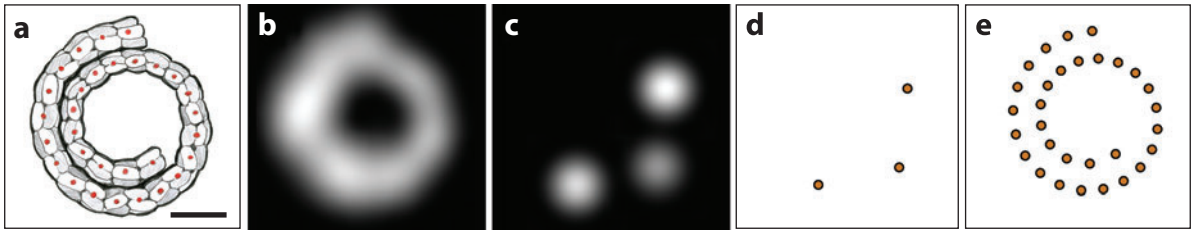

Figure 1

Schematic illustration of localization-based superresolution imaging. (*a*) A hypothetical object with spatial structure at scales smaller than the wavelength of light. Orange circles indicate fluorophores. (*b*) Conventional fluorescence imaging of the structure in panel *a*, with diffraction making the fine structure unresolvable. (*c*) Fluorescence imaging of a stochastically activated subset of the fluorophores. (*d*) Image analysis revealing the positions of the fluorophores in panel *c*. (*e*) Repeated imaging of sparse subsets of fluorophores, ideally yielding the positions of all the fluorophores and thereby providing superresolution imaging of the object. In panels *b* and *c*, pixelation and noise are not depicted. The scale bar is half the wavelength of the imaged light.

finer than Δ. As we discuss below, detecting N photons allows measurement of the PSF center with precision $\Delta/\sqrt{N}$. The accuracy required for characterizing the Brownian dynamics of colloidal tracer particles (11), or measuring the few nanometer steps of single kinesin proteins (3), for example, is readily attainable from imaging-based single-particle tracking experiments.

As realized by Betzig (12) in the mid-1990s, accurate single-fluorophore localization can be applied to systems of many fluorophores densely labeling a specimen, enabling microscopy beyond the diffraction limit, if these fluorophores can be imaged sequentially as isolated point sources. Let us consider, for example, the emitters in **Figure 1**, many of which are separated by less than Δ. Imaged concurrently, they produce a blur that obscures their spatial arrangement. If a molecule emits light while the others near it are dark, however, its position can be precisely determined (**Figure 1*c*,*d***). If one collects a series of images of sparse subsets of molecules and localizes each individual image's position, the arrangement of all the fluorophores is revealed (**Figure 1*e***). Implementing this elegant idea requires fluorescent probes that are not constantly emitting light, whose photophysical states can be switched so that only a small fraction of molecules are detected at any instant in time. A decade passed before this technical challenge was met. In 2005, Lidke et al. (13) showed that the stochastic emission of quantum dots can enable localization-based superresolution microscopy. In 2006, three groups, including Betzig and colleagues, demonstrated active control of molecular emission, using photoactivatable fluorescent proteins (4, 5) and photoswitchable organic fluorophores (6), yielding practical localization-based superresolution microscopy for biological imaging. Each group introduced a different name for the method—photoactivated localization microscopy (PALM) (4), fluorescence photoactivation localization microscopy (FPALM) (5), and stochastic optical reconstruction microscopy (STORM) (6)—and the years since have seen a continued proliferation of related methods and acronyms (14–16).

Localization-based superresolution microscopy has been performed using a wide variety of fluorophores, including both small organic molecules, such as cyanine dyes, and genetically encoded fluorescent proteins, such as photoactivatable variants of green fluorescent protein. The former typically have greater brightness and hence yield better localization precision; the latter allow noninvasive imaging via their expression in live cells. Comparisons of different fluorescent probes and related discussions can be found in other reviews on superresolution imaging (9).

Since 2006, localization-based superresolution imaging has been applied to a wide variety of biological systems. These include cytoskeletal networks, mitochondria, and focal adhesion complexes (4, 17–19). In addition, the technique has been extended to provide high-resolution three-dimensional (3D) positional information, which we discuss below.

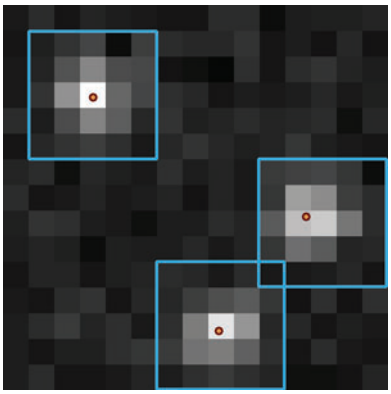

Figure 2

Simulated CCD image of three fluorophores (wavelength 530 nm, scale 100 nm/pixel, and $N \approx 400$ photons). Orange circles indicate the true fluorophore positions. Blue lines show 5 × 5 pixel regions of interest centered at the three brightest local intensity maxima.

Localization-based methods are not the only route to superresolution microscopy. Other techniques have emerged in recent years, most notably stimulated emission depletion microscopy (20, 21), in which fluorophore emission is optically manipulated to create a narrow PSF, and structured illumination microscopy, in which spatially patterned illumination and appropriate postprocessing allow superresolution reconstruction (22, 23). We do not further discuss these methods here, as their implementation and analysis are very different from those of localization-based techniques. We note, however, that a key advantage of localization-based superresolution imaging, beyond high resolution, is that it is relatively easy to implement on standard fluorescence microscopes, not requiring specialized optical equipment.

In the following sections we explore in detail the localization of single molecules in images, the precision of which determines the quality of a superresolution reconstruction, considering both fundamental limits and practical implementations.

3. FUNDAMENTAL LIMITS ON LOCALIZATION ACCURACY

How accurately can the location of a light-emitting molecule be determined? Typical CCD (charge-coupled device) images of single molecules look like those shown in **Figure 2** and are produced by some finite number of photons interacting with a pixelated, noisy detector. From its image, we wish to estimate the position of a light-emitting molecule.

The PSF gives the probability distribution of photon arrival positions at the detector, and hence the observed intensity distribution, and typically takes the form of an Airy disc:

$$p_0(r, r_0) = \left[\frac{2J_1(a|r - r_0|)}{a|r - r_0}\right]^2, \tag{1}$$

where $a = 2\pi \mathrm{NA}/\lambda$, J_1 is the first-order Bessel function of the first kind, $r_0 = (x_0, y_0)$ is the true position of the molecule, and r is a 2D position vector. Often, for simplicity, this distribution is approximated by a 2D Gaussian. The joint probability distribution governing the detection of N photons is

$$p(r, r_0) = \prod_{i=1}^{N} p_0(r, r_0) = (p_0(r, r_0))^N. \tag{2}$$

A more exact expression accounting also for the randomness inherent in the photon count can be found in Reference 24.

We wish to know how well any estimator for r_0 that we might construct will perform (i.e., the variance of our estimate, $\hat{r}_0$, about the true value, r_0). This general statistical question has a well-defined answer (24, 25): The minimum possible variance in $\hat{r}_0$, known as the Cramer-Rao lower bound (CRLB), is inversely proportional to the Fisher information matrix **I**. Elements of the information matrix are proportional to the number of independent measurements (N) and depend also on the shape of the probability distribution, being roughly inversely proportional to the squared width of the distribution (σ^2). Hence one would expect that the localization precision, δ, the square root of the variance, must satisfy $\delta \geq \sigma/\sqrt{N}$. For a 2D probability distribution, the matrix **I** is given by

$$I(r_0) = \begin{bmatrix} -E\left[\frac{\partial^2 \ln p(r;r_0)}{\partial^2 x}\right] & -E\left[\frac{\partial^2 \ln p(r;r_0)}{\partial x \partial y}\right] \\ -E\left[\frac{\partial^2 \ln p(r;r_0)}{\partial x \partial y}\right] & -E\left[\frac{\partial^2 \ln p(r;r_0)}{\partial^2 y}\right] \end{bmatrix}, \quad (3)$$

where E denotes the expectation value, and the derivatives are evaluated at the true value (x_0, y_0).

For a radially symmetric PSF, the off-diagonal elements of **I** are zero and the diagonal elements are equal. Hence the best possible localization precision in the x dimension is given by

$$\partial_x = \sqrt{\mathrm{var}(\hat{r}_x)} \geq (I_{xx})^{-1/2} = \left(-E\left[\frac{\partial^2 \ln p(r;r_0)}{\partial^2 x}\right]\right)^{-1/2}, \quad (4)$$

and similarly for y.

If we neglect pixelation and extrinsic noise, the above expression for **I** reduces to a simple, analytically tractable form for an Airy function PSF, giving the following bound on localization precision (24):

$$\delta_x = \delta_y = \frac{\lambda}{2\pi \mathrm{NA}\sqrt{N}}. \quad (5)$$

Similarly, a Gaussian PSF of width σ_g also yields a simple solution: $\delta_{\mathrm{X,Gaussian}} = \delta_{\mathrm{Y,Gaussian}} = \sigma_g/\sqrt{N}$.

For typical experiments, $\lambda \approx 500$ nm, NA ≈ 1.4, and $N \approx 100$–10,000 photons, determined by the camera exposure time, detection efficiency, and the fluorophore, so the fundamental limit on localization precision is ≈0.6–6 nm in each dimension. The overall root-mean-squared localization error for an isotropic 2D fluorophore image,

$$\delta_{\mathrm{CRLB}}^{\mathrm{fundamental}} = \delta_x \sqrt{2}, \quad (6)$$

spans ≈1 to 10 nm (**Figure 3*a***).

Pixelation and noise alter the experimental probability distribution and further limit the attainable localization precision. Typical CCD pixel sizes of approximately 6 μm and objective magnifications of 60× give typical image scales of 100 nm per pixel—significant compared to the PSF width. Typical noise sources are Poisson distributed (e.g., shot noise intrinsic to random photon emission) or Gaussian distributed (owing to camera readout circuitry). All these factors can be incorporated into the information matrix, leading to more complex but still tractable expressions for the bounds on localization precision (24). As an example, **Figure 3*a*** shows the limits on precision, δ_{CRLB}, for the example wavelength and numerical aperture given previously, with Poisson-distributed noise and a region size of 7 × 7 pixels at 100 nm/pixel. Ober and colleagues (26) have provided a useful online tool for calculating the CRLB for user-input imaging and noise parameters; alternatively, one can determine it from simulated images using Equations 1–4.

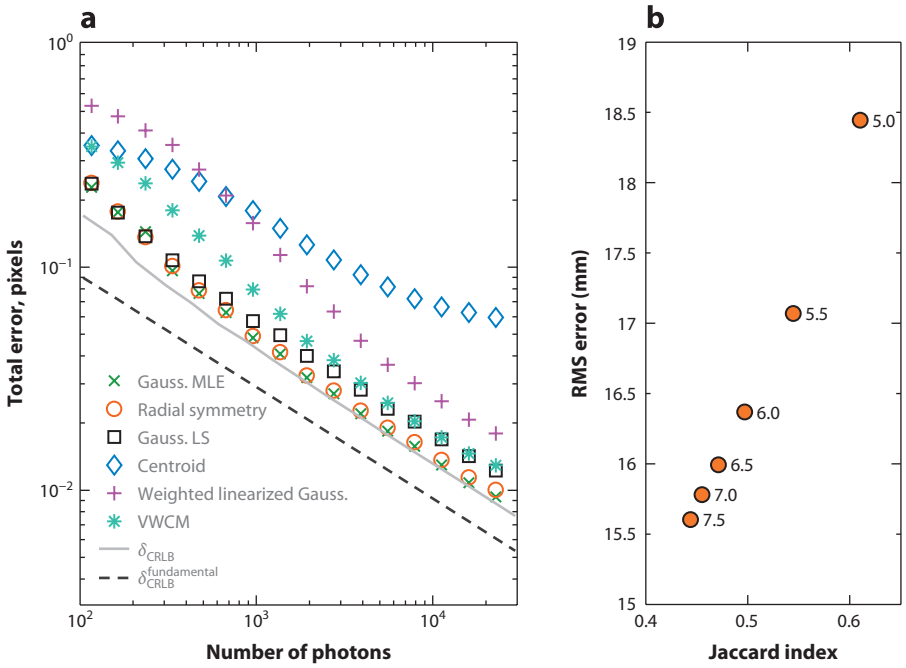

Figure 3

(*a*) Fundamental limits on localization accuracy and performance of several localization algorithms, as a function of the detected number of photons. The dashed and solid lines indicate the Cramer-Rao lower bounds (CRLBs) in the absence and presence of pixelation and noise, respectively. Each data point indicates the root-mean-squared (RMS) localization error from 1,000 simulated 7×7 pixel images of single fluorophores with locations randomly distributed over ± 0.5 pixels from the image center, with $\lambda = 530$ nm, NA = 1.3, scale 100 nm/pixel, Poisson-distributed noise, and additional background noise equivalent to 10 photons. Abbreviations: MLE, maximum likelihood estimation; LS, least squares; VWCM, virtual window center of mass. (*b*) Localization error versus Jaccard index for a set of simulated superresolution microscopy images, assessed with radial symmetry–based localization applied to regions of interest identified as local maxima with an intensity some number of standard deviations above the median. The number by each data point indicates the standard deviation threshold. The trend, of greater accuracy (lower RMS error) but worse recall (lower Jaccard index), for more selectively chosen regions applies generally to superresolution analysis.

Statistical bounds on localization accuracy set the fundamental limits on how well single-molecule positions can be estimated and provide a useful starting point for experimental analyses. They do not, however, provide a means for actually estimating these positions. Moreover, one should remember that these bounds describe the variance in position estimates, which reflect the measurement accuracy only if the estimation method is free of systematic biases (e.g., toward or away from the centers of image pixels).

4. LOCALIZATION METHODS AND THEIR ASSESSMENT

For most practical purposes, particle localization algorithms can be categorized by four criteria: (*a*) fitting a PSF model to the data versus estimating positions without explicit fitting, (*b*) analyzing single-molecule images versus analyzing overlapping images of several fluorophores in close proximity, (*c*) analyzing in two dimensions versus three dimensions, and (*d*) employing methods that assume fixed dipoles versus those that assume freely rotating dipoles. We largely focus on

2D localization of freely rotating dipoles for two reasons. First, such methods are more mature than those for localizing fixed dipoles or for localizing freely rotating dipoles in three dimensions. Indeed, in many cases, the issue of dipole orientation is completely irrelevant, either because single molecules can rotate freely during the image acquisition time or because the specimen is labeled with many randomly oriented molecules. Second, the most rigorous approaches to the localization of fixed dipoles and 3D localization involve fitting PSF models, and many key issues from the 2D localization of freely rotating dipoles also apply to the fixed and 3D cases.

The accuracy of localization algorithms is typically assessed by tests on simulated images containing single light-emitting molecules. Such images are straightforward to produce (27). Convolution of a point-like source with the PSF gives a PSF centered at the emitter location (x_0, y_0). By partitioning this intensity profile into pixels and incorporating noise, one can mimic CCD detection. Noise models typically represent Poisson-distributed shot noise and constant or Gaussian-distributed readout noise (28). For the former, one draws the intensity of each pixel from a Poisson distribution of a mean equal to the number of photons detected at that pixel (which is proportional to the PSF), and for the latter, an additional constant or random value is added. The resulting simulated image can then be assessed by the localization algorithm of interest, and the resulting estimated particle center (x_c, y_c) can be compared with the true position (x_0, y_0). The root-mean-squared error, $\sqrt{\langle |dr|^2 \rangle}$, where $dr = (x_c - x_0, y_c - y_0)$ and the brackets indicate an average over many simulated images, may itself be a function of (x_0, y_0) if the localization method is biased. For an unbiased estimator, the root-mean-squared error is clearly equal to the square root of the variance of dr, and its minimum possible value is constrained by the CRLB described above.

4.1. Prelocalization Tasks

Before a localization algorithm is applied to the data, essentially all analysis approaches identify regions of interest (ROIs) by drawing windows around pixels that are brighter than their neighbors and that exceed the expected background level in the image by some amount (**Figure 2**) (29–33). (Background is generally estimated from averages of dim regions.) However, even if a local brightness maximum is indeed near the approximate position of a fluorescent source, that bright pixel might not coincide with the exact fluorophore position (**Figure 2**). When the algorithm uses an approximate PSF model, this can be a problem, especially if there are large discrepancies between the model and the true PSF in the tails of the image. An off-center ROI means that in some significant portion of the ROI, the PSF model will be a poor approximation. Tail issues can be especially problematic when fitting the data to a Gaussian, which decays exponentially, as real PSFs tend to decay more slowly, especially with aberrations. Consequently, some algorithms [e.g., M2LE (34)] will draw several ROIs around a bright spot (e.g., one ROI for each pixel that exceeds the background noise by a given threshold, regardless of whether it exceeds its neighbors). This gives several position estimates (one per ROI); the estimate that is closest to the center of its ROI is taken to be the position of the molecule. However, a centered molecule is obviously necessary only for algorithms that assume single-molecule images. When working with multimolecule images, it will be impossible for all estimates to be centered, and even the requirement that the molecules at least cluster away from the edges of the ROI may be impossible.

4.2. Discrimination of Multiparticle Regions

When using a single-molecule localization algorithm (as opposed to one that can handle several overlapping images of molecules in close proximity), one must also determine if the image is indeed of a single molecule rather than several. In some cases, the photon count is a sufficient discriminator. If the brightness of a single-emitter image is well known (i.e., the quantum efficiency

is not variable and the distribution of on times is well characterized), then images well above the expected number of photon counts may be discarded, especially if tracking steady emitters (35). Even for blinking emitters, whose on times are usually exponentially distributed (6), images at 3× the expected brightness, for example, have only a 5% chance of being from a single molecule. When the photon count is not a sufficient discriminator, a shape test may work well: Overlap images tend to be elliptical, and tests of shape are less computationally complex than iterative fits to a PSF model. Finally, sometimes the test of the single-molecule model is indirect; if the localization algorithm fails to converge, or returns a residual or likelihood score that is above some user-defined threshold, the image may be rejected.

A rejection step prior to localization is important for experimental design as well as data analysis. Because of the stochastic nature of the activation and blinking processes in superresolution localization microscopy, one generally has no control over which fluorophores are activated, only the fraction that is activated. If the activation probability per molecule is too low, many frames contain no activated molecules, which represents a wasted opportunity to collect data. If the activation probability per molecule is too high, most frames will contain multimolecule overlaps rather than single-molecule images. The consequence is that increasing the activation probability actually decreases the number of useful images and hence slows down the experiment (36). At the optimum activation probability, the ratio of two-molecule images to single-molecule images is 0.5, which means that a substantial portion of the bright spots is not suitable for single-molecule analysis. Consequently, a rejection step is necessary prior to localization.

Of course, rejection algorithms do not always correctly identify the single-molecule images. Noise might distort a single-molecule image such that it fails a stringent shape test, and some two-molecule images might result from molecules so close to each other that the shape is nearly circular. Consequently, rejection algorithm performance is characterized by two key parameters: the fractions of single-molecule and two-molecule images accepted and passed along for localization (f_1 and f_2, respectively). At the optimum activation probability, the maximum ratio of accepted two-molecule images to accepted single-molecule images is $f_2/2f_1$ (36). If this error rate is not acceptable, it can be reduced by working with a lower activation probability. Additionally, in many linear structures (e.g., parallel tubes), the most likely overlaps are from two molecules either on the same tube (in which case a localization algorithm will return a position that is intermediate between them and hence still on the structure, thus presenting real information) or on different lines (in which case the spacing will be larger, the image will be elliptical, and the odds of rejection may be high) (**Figure 4**).

Issues of rejection in three dimensions or with fixed dipoles (and the consequences thereof) have been less explored. Images of dipoles tend to be asymmetric, and the photon counts are more variable (depending on the overlap between the emission pattern and the collection angle of the microscope), making it harder to do shape-based or brightness-based rejection. The best option is to fit to a good model and reject images with low likelihood scores or large residuals. In 3D localization, the axial coordinate can be estimated by a number of different methods, and the expected shape and even brightness of a single-molecule image depend on the 3D technique used. It is challenging to conceive of rejection algorithms based on anything other than very poor fit to the expected model.

4.3. Fitting-Based Methods

Fitting-based localization uses knowledge of the approximate PSF and noise in the imaging system. The PSF generally has four to five parameters: the emitter coordinates (x_0, y_0), a parameter proportional to the photon emission rate by the emitter (denoted I_0), a background level b, and perhaps a width w (which depends on the wavelength of light and degree of defocus). For an

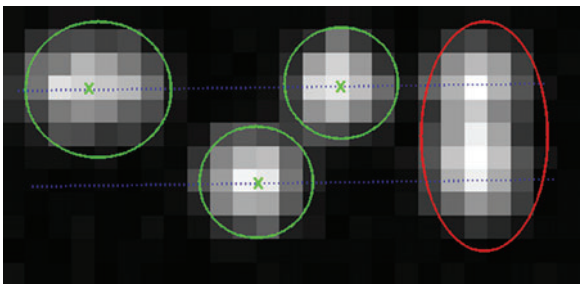

Figure 4

An example of the effect of a rejection algorithm on the analysis of parallel linear structures (*dashed blue lines*) with sparsely activated labels (simulated images). Six fluorophores are activated, forming two overlap spots (*left and right ellipses*) and two single-molecule spots (*center circles*). The circles and the less eccentric ellipse are accepted (*green*), and from those images three molecular positions are estimated (*green crosses*). The more eccentric ellipse is rejected, and no position estimate is returned. Although one of the accepted images is in fact a two-molecule image, the resulting position estimate still lies on the structure of interest, so there is no negative effect on the final reconstruction.

isotropic emitter, the signal can be written as

$$S(x, y) = b + I_0 b \left(\frac{\sqrt{(x - x_0)^2 + (y - y_0)^2}}{w} \right) + \text{noise}.$$

The first two terms are the expected signal; the noise is a random variable. The fitting algorithm minimizes discrepancies between the model and the signal, by picking the appropriate parameter values.

There are two common methods for minimizing the discrepancy between model and signal: least squares and maximum likelihood estimation (MLE). Least squares is intuitive: For given parameter estimates, one computes the difference between the signal and model on each pixel, squares the errors, and adds them. One then picks new parameter estimates and again computes the sum of the squared errors to see if the new parameter values improve the error. One iteratively varies the estimates until the sum of squared errors is minimized.

MLE is somewhat less intuitive and requires more detailed information about the experimental system. However, the theorem of Cramer and Rao states that MLE gives the most precise estimates when one has good models for the PSF and noise (25, 37). One again computes the difference between the signal and model and then uses the statistics of the noise to predict the likelihood of that difference. Small differences are more likely than large differences, so small discrepancies have a high likelihood. The parameters are varied to maximize the likelihood of the data.

The advantages of MLE are that (*a*) a mathematical theorem states that the estimates from MLE have the theoretical minimum variance (in the limit of large *N*), and (*b*) the precise value of that variance, the CRLB, can be calculated from the Fisher information matrix discussed above. The desirability of minimum variance and unbiased position is obvious. The value of the variance being known is that it gives a means for checking the performance of a system: One can image the same emitter(s) repeatedly, use MLE to determine the position(s), and compute the variance of the estimates from the localization analysis. If the variance is close to the CRLB, then one likely has a valid model for the PSF and noise in the system. If, however, the variance differs substantially from the CRLB, there is a problem with one or more aspects of the model. Tests on realistic noisy, pixelated images show that fitting Gaussian or Airy function PSFs by MLE provides the most accurate known localization approach, as described in detail in References 27 and 38, with unbiased performance and precision close to the CRLB (**Figure 3*a***).

The biggest drawback of MLE is that it requires a well-characterized noise model. When additive read noise is significant, the combined Gaussian/Poisson distribution can be complicated to work with (24). Likewise, Poisson noise is just an approximation when working with an EMCCD (electron multiplying charge-coupled device) (39). Highly optimized software packages do exist to perform MLE with these noise models (39, 40). However, the package optimized for EMCCDs is designed for very high magnification, whereas the package optimized for sCMOS (scientific complementary metal oxide semiconductor) cameras works best if one has a good pixel-by-pixel measurement of read noise. Fortunately, many MLE implementations work well with approximate PSFs and a shot noise model, including a GPU (graphics processing unit) implementation (33) and one optimized to reduce run time on a single processor (41). Several other integrated packages also include MLE (e.g., 42).

The biggest advantage of least squares is that it is simpler to implement and requires less information than MLE. Additionally, in the limit of large photon counts, the Poisson noise approaches a Gaussian distribution, and for pure Gaussian noise, the maximum likelihood and least-squares criteria are mathematically equivalent. In practice, for realistic imaging conditions, fitting by least-squares minimization performs nearly as well as MLE (**Figure 3*a***) (27). One particularly noteworthy implementation of least squares is for 3D biplane localization (43) with measured PSFs: In biplane imaging, two images are taken with different focal depths, and the relative widths of the images can be used to estimate the z coordinate. Given the importance of properly calibrating the PSF's depth dependence, it can be advantageous to use an experimentally measured PSF rather than an approximate analytical formula. Additionally, a fast iterative implementation of least squares exists: Gaussian mask (44).

One must take care with the tails of the PSF: Statistical theory recommends that squared errors be weighted by the expected variance of the error, which is the expected signal in the case of Poisson noise. However, this prescription is valid only if one has a good model for the signal. The Gaussian PSF model works well near the center, but it decays rapidly in the tails, leading to a potential small denominator problem. This is not an issue with an experimentally measured PSF (43), but it may be an issue with an approximate PSF. Consequently, many least-squares implementations do not weight the errors and instead weight all errors equally (42). Also, in weighted least-squares implementations, it is important to not use the signal to weight, as the signal is subject to noise and may exhibit a downward fluctuation, worsening the small denominator problem, but rather to use the expected signal, whether from a measured PSF or an experimentally validated analytical formula (38).

Moreover, if one neglects the additive background in the tails, one could convert the fitting of a Gaussian PSF into a linear least-squares problem (45):

$$\log\ \text{signal} = \log I_0 + w_x(x - x_0)^2 + w_y(y - y_0)^2,$$

with fit parameters w_x, w_y, x_0, y_0, and I_0. This fitting problem can be solved analytically (without iteration). However, this approach is highly sensitive to errors in the tails, both because of the inevitable mismatch between an exponentially decaying Gaussian and real data and because the logarithm will magnify small discrepancies. Unless the signal/noise ratio is extremely high and the Gaussian PSF is a well-validated approximation for the imaging system, this linearized Gaussian approach leads to poor accuracy (**Figure 3*a***) and is not recommended.

4.4. Methods that Do Not Require Fitting

The mathematical strength of fitting-based methods is their ability to incorporate information about the PSF and camera noise. However, that strength is also a weakness, requiring the user

to have detailed information. This is especially problematic when imaging deep in a complex and inhomogeneous sample. Additionally, fitting techniques can be computationally intensive, requiring many function evaluations for each pixel and each iteration. The test images in **Figure 3*a***, for example, were localized with an average computation time per image two to three orders of magnitude greater for MLE or least-squares fitting than for the nonfitting-based methods described below. To surmount this limitation, researchers have developed a variety of approaches. Starr et al. (41) have shown that the separation of a Gaussian PSF into radial and angular components yields computation times that scale as the square root of the number of pixels in the image, rather than linearly, and Smith et al. (33) have demonstrated that using GPUs for fitting can speed up localization by up to a factor of 100. Although GPU computing is becoming more widespread, computational simplicity is still a desirable attribute if one wishes to do the processing on chip or on a mobile device for microscopy in the field (46).

The simplest but most problematic nonfitting method is centroid analysis. The biggest flaw of centroid analysis is that it is very sensitive to uniform additive background noise, which biases the estimate toward the center of the ROI (31, 47, 48). Filtering can reduce the background intensity and thereby improve the performance of centroid methods (49). However, a more robust fix is to iteratively redraw the ROI to keep the centroid estimate centered in the window, reweighting the signals of edge pixels as needed (47). This virtual window center of mass approach considerably improves the localization accuracy of centroid finding (**Figure 3*a***) and can provide a good seed value for iterative fitting techniques.

A promising nonfitting technique is the radial symmetry algorithm, which works on the principle that, irrespective of the specific PSF shape, the image will be (aside from noise) radially symmetric if the emission pattern is isotropic. This is a very minimal assumption, making the algorithm suitable for use in a wide range of circumstances. The localization precision of this algorithm has been compared with the CRLB and typically comes quite close (in a single iteration!) for realistic photon counts, noise, and PSF shapes (31) (**Figure 3*a***). Moreover, its simplicity makes it suitable for on-chip implementation with field-programmable gate arrays (50). Unlike MLE, this symmetry-based approach has not been exhaustively analyzed; it is not evident why it works as well as it does, and elaboration would likely aid future algorithm development.

4.5. Estimation of Fluorophore Positions from Multifluorophore Overlap Images

As long as one is restricted to single-emitter localization, there is a maximum activation probability, past which activating more molecules replaces single-molecule images with multimolecule images. However, if one could extract information from multiemitter overlap images, then one could activate more molecules per frame and thus localize more molecules more rapidly. This speed enhancement requires algorithms that can solve the inverse problem for a multiemitter overlap image. The greater the number of emitters that the algorithm can handle simultaneously, the greater is the speed improvement. If, for instance, an algorithm can handle up to six molecules in a diffraction-limited spot, the potential speed improvement in the experiment is approximately a factor of eight (36).

The most mathematically rigorous way to fit a multiemitter model to the data is still MLE. This requires a good model for the camera noise and the PSF and can be mathematically complex. It does, however, deliver minimum-variance position estimates. Software that does the multiemitter MLE fit is available, can be implemented on a GPU, and has been optimized for read noise in sCMOS cameras (30, 40). In direct comparisons (51), a multiemitter MLE approach, PALMER (51, 52), compared favorably with a least-squares package, DAOSTORM

(29). However, multiemitter least-squares fits are also possible and have the usual advantages of least squares over MLE: They are often simpler, and they require less information. There is a version of DAOSTORM that works well with 3D data (53). In many 3D superresolution techniques, one inserts a cylindrical lens into the system to introduce astigmatism; the resulting image is elliptical, with an eccentricity that depends on the z coordinate and an orientation (vertical or horizontal) that depends on the sign of z. 3D DAOSTORM models the data as a superposition of elliptical PSFs and fits the model via least squares.

4.6. Estimation of Density from Multifluorophore Overlap Images

Not every approach to multiemitter images involves position estimation. There are several interesting algorithms that estimate a density of molecules rather than molecular positions. Although single-molecule resolution is not sought, the density maps often have spatial frequencies substantially larger than $1/\lambda$ and are thus superresolution images. Individual methods have strengths and weaknesses, but one common advantage is that they draw from data-analysis approaches used in many other fields of science and engineering. The exploration of these techniques by the superresolution, single-molecule, and particle-tracking communities likely will lead to useful exchanges of ideas.

Among density map approaches, three have gained special attention. DeconSTORM (54), based on deconvolution, is effectively an MLE approach for density maps: It picks the density map that maximizes the likelihood of the data given a model for the PSF, noise, and (when the emitters are switchable molecules) blinking dynamics. Compressed sensing, another approach, requires less information (just a PSF, no noise model) (55). The basic idea is that the problem of estimating a subpixel structure is underdetermined because there are fewer pixels than features. Many different maps of molecular density are thus consistent with the data; the goal is to pick the sparsest structure (i.e., the greatest number of zeros in the density map) that is consistent with the data. Because this technique generates an image, typically on a subpixel grid, rather than a list of molecule positions, comparison with localization algorithms is not straightforward. However, as Zhu et al. (55) demonstrated, an effective localization precision can be inferred from the reconstructed image, and this precision exceeds that of single-molecule fitting for densities greater than a few molecules per square micrometer.

A very different approach is based on Bayesian statistics (56). The algorithm identifies not a single underlying structure, but rather a probability-weighted superposition of structures. The biggest advantage is that it considers the entire sequence of images, rather than just individual images. Although there is a computational cost, the algorithm can be sped up via cloud computing (57). Because this method is rooted in Bayesian statistics, there are intriguing possibilities for modifying the algorithm to use prior information. For instance, if one labels the cytoskeleton, one would expect an image whose Fourier spectrum is dominated by two frequencies: the inverse of the fiber width and the inverse of the characteristic fiber spacing. Reconstructions that satisfy this property could then receive greater weight.

4.7. Dipole Orientation

All the above methods treat the emission profile of a single molecule as isotropic, giving a radially symmetric blur at the image plane. However, the true intensity distribution of a light-emitting molecule is that of a radiating electric dipole, the shape and isotropy of whose projection onto the imaging plane will depend on the dipole orientation. Significantly, the intensity maximum need not correspond to the image center and molecular position. Typically, the rotational freedom of molecules and the low-pass filtering of the lens aperture blur away anisotropy. However, dipole

orientation can provide useful information on macromolecular orientation (58). Moreover, if the dipole orientation is fixed, single-molecule localization by Gaussian fitting or any other isotropic approach will lead to localization errors. For typical wavelengths and imaging conditions, these errors can be tens of nanometers for fixed molecules situated in the imaging focal plane, and up to approximately 200 nm for molecules several hundred nanometers away from the focal plane (59–61). Mortensen et al. (38) fitted the dipolar PSF to analyze the position and orientation of molecules at the focal plane. Aguet et al. (62) have shown that the use of a defocused image and a steerable filter allows the assessment of dipoles at a known nonzero distance from the focal plane. Backlund et al. (59) recently provided an elegant and general approach to the issue of determining dipole position and orientation, using a phase mask to shape their PSF into a double-helical form. With this, the emission of a single dipole appears as two lobes, the midpoint of which gives the *xy* position of the molecule and the angle of which gives the position in *z* (63). If the molecule were to translate in *z*, the image would trace out a double helix. The problem of localizing a dipole is therefore transformed into that of localizing two roughly symmetric spots, which is then amenable to the methods detailed above.

In terms of methodological innovation, the fundamental issue involves models rather than algorithms. With an adequate model for the emission pattern of a fixed dipole imaged in a given hardware setting, the most mathematically rigorous approach is MLE of the molecule's coordinates. However, this requires either a rigorous model from vectorial diffraction theory (taking into account the finite numerical aperture of the imaging system and reflection and refraction at the various interfaces in the system) or a suitable approximation to such a model (e.g., expanded in a mathematically convenient basis) (64). A bigger problem is how to handle a dipole that is not fixed (i.e., rigorous vectorial diffraction theory is not useful) but not completely free (i.e., isotropic approximations cannot be used). In particular, what if the molecule's rotational motion is subdiffusive? Is there a useful fitting model? Is there at least some image property that depends on molecular position but not on dipole orientation? Given the success of the radial symmetry method, which starts from the fact that an isotopic emitter can be expanded in radially symmetric functions ($m = 0$ in the language of spherical harmonics), one might ask if a useful algorithm could be constructed from some invariant of the dipole PSF. The signal from a rotationally diffusing (or subdiffusing) dipole is a superposition of different functions with nonzero m but $l = 1$ (in the language of spherical harmonics). It is worth asking what invariants might exist for such superpositions, and whether a useful localization algorithm could be constructed from that insight.

4.8. 3D Superresolution Issues

From an image analysis perspective, 3D superresolution methods (much like imaging of fixed dipoles) pose issues of models rather than algorithms. For every widely used 3D superresolution technique, 3D information is obtained by fitting the data to a model with a parameter that encodes the *z* coordinate. In astigmatism-based imaging (65), the model is simply an elliptical Gaussian, and good MLE routines exist with GPU implementations (33). In biplane imaging, the *z* coordinate is inferred by comparing the widths of the blurs in images focused on two different planes, and as long as the relationship between the defocus and PSF width is well characterized, the position estimation is straightforward (66). Fitting routines have been developed that use experimentally measured PSFs for this task (67). In the case of imaging with a two-lobed PSF, the models are more complex, but MLE can still be applied. The key theoretical point to keep in mind is that 3D imaging with the two-lobed PSF has been shown to have a better theoretical limit to localization precision for all three coordinates because the main effect of defocus is to rotate the PSF rather

than broaden it (68, 69). However, a user needs to weigh the theoretical advantages against the greater hardware complexity.

4.9. Assessment of Localization Methods Using Many-Particle Images

Real images obtained in superresolution microscopy studies typically contain several molecules, some of which may be brighter or dimmer than others, and some of which may be close to one another, all superimposed on backgrounds of possibly spatially varying intensities. No single measure can capture the performance of any analysis protocol, as analysis requires both identification of candidate particles and localization of particle position. These two tasks are coupled: Focusing on bright particles (large numbers of photons) yields high-precision localization but at the cost of ignoring the contribution of dimmer molecules to the image reconstruction. Conversely, a low brightness threshold for selection gives more points for reconstruction but at the cost of lower precision per point and a greater rate of false-positive identification of noise as molecules. Many metrics characterizing molecule detection are possible. Given simulated data sets of known positions, a useful one (32) is the Jaccard index (J), which characterizes the similarity of the sets of detected and simulated particles, calculated as

$$J = \frac{N_{TP}}{N_A + N_B - N_{TP}},$$

where N_A and N_B are the number of detected and simulated particles, and N_{TP} is the number of true positives [i.e., detected particles that lie within some radius (e.g., 100 nm) of a simulated particle]. **Figure 3*b*** illustrates this for a data set of simulated images analyzed using the radial symmetry–based localization described above applied to regions selected by finding local intensity maxima that are some number of standard deviations above the mean. As expected, the root-mean-squared error and J are strongly correlated with each other. It is important to be aware of this correlation for whatever analysis tools are being applied to superresolution data sets.

To provide useful benchmarks for the testing of superresolution software, a group associated with the 2013 International Symposium on Biomedical Imaging generated realistic simulated images that serve as a publicly available reference. This group also organized a challenge under which nearly 30 other groups applied their analysis software on the same simulated images (70). These images mimicked fields of microtubules and consisted of data sets with low and high densities of imaged emitters, with roughly 20 and 200 fluorophores per square micrometer of specimen per 2D image, respectively. The performance of various localization approaches roughly mirrored the discussion of particular algorithms above and will be discussed in detail in a publication from the organizers.

5. VISUALIZATION OF SUPERRESOLUTION RECONSTRUCTIONS

The output of localization microscopy is a list of estimates of single fluorophore positions and their uncertainties. One typically wants to turn this list into an accurate and informative image. This is a nontrivial task (71), in large part because of the resolution of a superresolution image being inherently nonuniform. Both the localization precision, which depends on particle brightness, and the sampling scale set by the labeling density determine the local resolution, with the latter often more important in practice (72).

The most common visualization approach is to create at each localized point a 2D Gaussian with width equal to the localization precision and construct the overall image as the sum of these Gaussians. This gives a reconstructed image whose intensity is linear in the density of fluorophores,

as desired for a fluorescence microscopy image. Moreover, its encoding of information on the localization precision provides a useful indication to the viewer of the reconstruction quality. However, this approach does not provide cues about the sampling-derived resolution and moreover degrades the overall resolution of the image because each point is blurred by the Gaussian width and also occupies a position that differs from the true (unknown) fluorophore position by an amount roughly equal to that width (71).

Alternatively, various groups have used 2D histograms to visualize localization microscopy data (71, 73). Again, this approach is linear in fluorophore density but does not indicate local resolution, as the bin size is fixed.

Recently, Baddeley et al. (71) have proposed two visualization approaches that maintain linearity but that indicate local resolution and preserve structure. These are a quad-tree-based adaptive histogram, in which quad-tree decomposition gives variable-sized 2D histogram bins, and visualization based on Delaunay triangulation, in which the size of triangles formed using localization data indicates the effective local resolution. It is not yet clear if these approaches will be widely adopted, but robust and well-motivated visualization methods are important, especially as localization-based microscopy is increasingly used for visual inference of subcellular structure.

6. CONCLUSIONS AND CHALLENGES

Although the principles and experimental implementation of localization-based superresolution imaging are well established, and algorithms for the localization of single molecules are, as detailed above, fairly well understood, there are still open issues that call for further work.

Compared to 2D imaging of symmetric PSFs, the analysis of nonspherical intensity distributions that arise in 3D localization microscopy and in imaging immobile dipoles is considerably less developed. Are there fast, effective ways of localizing anisotropic shapes? For dipoles, for example, is an exact treatment of emission PSFs necessary, or can we devise high-performing approximations that take advantage of the properties of $l = 1$ spherical harmonic intensity profiles convolved with a PSF? For dipoles, and especially for astigmatism-based 3D imaging, can we exploit the fact that intensity profiles, while not radially symmetric, possess other symmetries?

In general, fitting by MLE provides the most accurate approach to localization, although at the cost of computation time compared to nonfitting approaches. MLE requires a detailed noise model, which can be tailored to the properties of the imaging system. Nonfitting approaches, which have the attribute of speed, generally do not explicitly involve noise models. Can we produce algorithms that do not involve fitting, and hence are very fast, but that are adapted to particular and possibly large noise levels? This becomes especially important given the advent of high-performance sCMOS cameras (40), which have fairly high levels of read noise, and which are already being used for superresolution imaging (74, 75).

Many questions remain regarding performance of multiemitter localization algorithms for the discrimination of closely separated molecules. What is the relationship between localization accuracy and the number of molecules being fit? Why do some methods perform better than others? Is there a practical limit to the number of molecules that can be discerned? How will this depend on the number of photons emitted by each molecule, their proximity, the window size that the fit is applied to, and so on? What are the fundamental bounds on precision? This issue extends to 3D superresolution, for which even less has been done regarding overlapping intensity profiles.

From superresolution data, one of course wishes to gain mechanistic insights into cellular function, which often involves conclusions about structures such as filaments or aggregates like protein clusters (18). These require robust assessment of the effects of the proximity between

molecules, noted above, but also accurate estimation of the identity of molecules: Were two closely situated spots that were detected at different times emitted by the same molecule that blinked or by different molecules? The answer, which will strongly influence conclusions about clustering and intermolecular interactions, requires models of fluorophore photophysical behaviors, and more work is needed on drawing structural inferences from superresolution data.

Localization-based superresolution microscopy is a fairly new approach to imaging that has attracted enormous interest across a wide swath of science, for a good reason: With optical wavelengths and unspecialized equipment, it reveals subcellular structure at scales previously thought unattainable. Already, abundant examples exist of cellular images with tens-of-nanometer resolution, and in principle, nanometer-scale resolution is possible given a sufficient number of photons, a stable imaging platform, and accurate localization. The last point is particularly important: Unlike traditional microscopy, the performance, speed, and robustness of computational tools are inherently inseparable from the generation of images. We expect therefore that the coming years will continue to see the elaboration of fascinating new computational algorithms.

SUMMARY POINTS

1. New methods for superresolution microscopy are both enabled and limited by the performance of algorithms that extract the positions of particles or molecules from diffraction-limited images.
2. The precision with which a position can be determined depends primarily on the number of photons collected and the amount of noise in the image.
3. Criteria for selecting and evaluating regions of interest that contain light emitters, prior to the application of precise localization algorithms, are important for determining the overall performance of localization-based microscopy.
4. The most common localization methods use models of isotropic light emitters, although methods also exist for other emitter types, such as dipoles.
5. The most accurate and mathematically rigorous approach to particle localization is maximum likelihood estimation, which can be used as a yardstick for assessing the performance of other approaches.
6. Most alternatives to maximum likelihood estimation are appealing because they are either computationally faster or require less information about the imaging context.
7. Methods that extract positions from overlapping multiemitter images are increasingly popular and offer advantages for experimental design.

DISCLOSURE STATEMENT

The authors are not aware of any affiliations, memberships, funding, or financial holdings that might be perceived as affecting the objectivity of this review.

LITERATURE CITED

1. Stetson PB. 1987. DAOPHOT: a computer program for crowded-field stellar photometry. *Publ. Astron. Soc. Pac.* 99:191–222
2. Sainis SK, Germain V, Dufresne ER. 2007. Statistics of particle trajectories at short time intervals reveal fN-scale colloidal forces. *Phys. Rev. Lett.* 99:018303

3. Park H, Toprak E, Selvin PR. 2007. Single-molecule fluorescence to study molecular motors. *Q. Rev. Biophys.* 40:87–111
4. Betzig E, Patterson GH, Sougrat R, Lindwasser OW, Olenych S, et al. 2006. Imaging intracellular fluorescent proteins at nanometer resolution. *Science* 313:1642–45
5. Hess ST, Girirajan TPK, Mason MD. 2006. Ultra-high resolution imaging by fluorescence photoactivation localization microscopy. *Biophys. J.* 91:4258–72
6. Rust MJ, Bates M, Zhuang X. 2006. Sub-diffraction-limit imaging by stochastic optical reconstruction microscopy (STORM). *Nat. Methods* 3:793–95
7. Sengupta P, Van Engelenburg S, Lippincott-Schwartz J. 2012. Visualizing cell structure and function with point-localization superresolution imaging. *Dev. Cell* 23:1092–102
8. Huang B, Bates M, Zhuang X. 2009. Super-resolution fluorescence microscopy. *Annu. Rev. Biochem.* 78:993–1016
9. Fernández-Suárez M, Ting AY. 2008. Fluorescent probes for super-resolution imaging in living cells. *Nat. Rev. Mol. Cell Biol.* 9:929–43
10. Patterson G, Davidson M, Manley S, Lippincott-Schwartz J. 2010. Superresolution imaging using single-molecule localization. *Annu. Rev. Phys. Chem.* 61:345–67
11. Crocker JC, Hoffman BD. 2007. Multiple-particle tracking and two-point microrheology in cells. *Methods Cell Biol.* 83:141–78
12. Betzig E. 1995. Proposed method for molecular optical imaging. *Opt. Lett.* 20:237–39
13. Lidke K, Rieger B, Jovin T, Heintzmann R. 2005. Superresolution by localization of quantum dots using blinking statistics. *Opt. Express* 13:7052–62
14. Sharonov A, Hochstrasser RM. 2006. Wide-field subdiffraction imaging by accumulated binding of diffusing probes. *Proc. Natl. Acad. Sci. USA* 103:18911–16
15. Burnette DT, Sengupta P, Dai Y, Lippincott-Schwartz J, Kachar B. 2011. Bleaching/blinking assisted localization microscopy for superresolution imaging using standard fluorescent molecules. *Proc. Natl. Acad. Sci. USA* 108:21081–86
16. Fölling J, Bossi M, Bock H, Medda R, Wurm CA, et al. 2008. Fluorescence nanoscopy by ground-state depletion and single-molecule return. *Nat. Methods* 5:943–45
17. Brown TA, Tkachuk AN, Shtengel G, Kopek BG, Bogenhagen DF, et al. 2011. Superresolution fluorescence imaging of mitochondrial nucleoids reveals their spatial range, limits, and membrane interaction. *Mol. Cell. Biol.* 31:4994–5010
18. Greenfield D, McEvoy AL, Shroff H, Crooks GE, Wingreen NS, et al. 2009. Self-organization of the *Escherichia coli* chemotaxis network imaged with super-resolution light microscopy. *PLoS Biol.* 7:e1000137
19. Shroff H, Galbraith CG, Galbraith JA, White H, Gillette J, et al. 2007. Dual-color superresolution imaging of genetically expressed probes within individual adhesion complexes. *Proc. Natl. Acad. Sci. USA* 104:20308–13
20. Hell SW. 2007. Far-field optical nanoscopy. *Science* 316:1153–58
21. Willig KI, Harke B, Medda R, Hell SW. 2007. STED microscopy with continuous wave beams. *Nat. Methods* 4:915–18
22. Gustafsson MG. 2000. Surpassing the lateral resolution limit by a factor of two using structured illumination microscopy. *J. Microsc.* 198:82–87
23. Gustafsson MG. 2005. Nonlinear structured-illumination microscopy: wide-field fluorescence imaging with theoretically unlimited resolution. *Proc. Natl. Acad. Sci. USA* 102:13081–86
24. Ober RJ, Ram S, Ward ES. 2004. Localization accuracy in single-molecule microscopy. *Biophys. J.* 86:1185–200
25. Kay S. 1993. *Fundamentals of Statistical Signal Processing*, Vol. I: *Estimation Theory*. Englewood Cliffs, NJ: Prentice Hall
26. Ward ES, Ober RJ. 2012. FandPLimitTool. *GUI-Based Software Module.* **http://www.wardoberlab.com/software/fandplimittool/**
27. Abraham AV, Ram S, Chao J, Ward ES, Ober RJ. 2009. Quantitative study of single molecule location estimation techniques. *Opt. Express* 17:23352–73
28. Snyder DL, Helstrom CW, Lanterman AD, Faisal M, White RL. 1995. Compensation for readout noise in CCD images. *J. Opt. Soc. Am.* 12:272–83

29. Holden SJ, Uphoff S, Kapanidis AN. 2011. DAOSTORM: an algorithm for high-density super-resolution microscopy. *Nat. Methods* 8:279–80
30. Huang F, Schwartz SL, Byars JM, Lidke KA. 2011. Simultaneous multiple-emitter fitting for single molecule super-resolution imaging. *Biomed. Opt. Express* 2:1377–93
31. Parthasarathy R. 2012. Rapid, accurate particle tracking by calculation of radial symmetry centers. *Nat. Methods* 9:724–26
32. Křížek P, Raška I, Hagen GM. 2011. Minimizing detection errors in single molecule localization microscopy. *Opt. Express* 19:3226–35
33. Smith CS, Joseph N, Rieger B, Lidke KA. 2010. Fast, single-molecule localization that achieves theoretically minimum uncertainty. *Nat. Methods* 7:373–75
34. Small AR, Starr R, Stahlheber S. 2013. molecule-localization-plugin; M^2LE: a molecule localization plug-in for ImageJ. *Software Plug-in.* **https://code.google.com/p/molecule-localization-plugin/**
35. Lagerholm BC, Averett L, Weinreb GE, Jacobson K, Thompson NL. 2006. Analysis method for measuring submicroscopic distances with blinking quantum dots. *Biophys. J.* 91:3050–60
36. Small AR. 2009. Theoretical limits on errors and acquisition rates in localizing switchable fluorophores. *Biophys. J.* 96:L16–18
37. Papoulis A. 1991. *Probability, Random Variables, and Stochastic Processes*. New York: McGraw-Hill
38. Mortensen KI, Churchman LS, Spudich JA, Flyvbjerg H. 2010. Optimized localization analysis for single-molecule tracking and super-resolution microscopy. *Nat. Methods* 7:377–81
39. Chao J, Ram S, Ward ES, Ober RJ. 2013. Ultrahigh accuracy imaging modality for super-localization microscopy. *Nat. Methods* 10:335–38
40. Huang F, Hartwich TMP, Rivera-Molina FE, Lin Y, Duim WC, et al. 2013. Video-rate nanoscopy using sCMOS camera-specific single-molecule localization algorithms. *Nat. Methods* 10:653–58
41. Starr R, Stahlheber S, Small A. 2012. Fast maximum likelihood algorithm for localization of fluorescent molecules. *Opt. Lett.* 37:413–15
42. Wolter S, Löschberger A, Holm T, Aufmkolk S, Dabauvalle M-C, et al. 2012. rapidSTORM: accurate, fast open-source software for localization microscopy. *Nat. Methods* 9:1040–41
43. Mlodzianoski MJ, Schreiner JM, Callahan SP, Smolková K, Dlasková A, et al. 2011. Sample drift correction in 3D fluorescence photoactivation localization microscopy. *Opt. Express* 19:15009–19
44. Thompson RE, Larson DR, Webb WW. 2002. Precise nanometer localization analysis for individual fluorescent probes. *Biophys. J.* 82:2775–83
45. Anthony SM, Granick S. 2009. Image analysis with rapid and accurate two-dimensional Gaussian fitting. *Langmuir* 25:8152–60
46. Zhu H, Yaglidere O, Su T-W, Tseng D, Ozcan A. 2011. Cost-effective and compact wide-field fluorescent imaging on a cell-phone. *Lab. Chip* 11:315–22
47. Berglund AJ, McMahon MD, McClelland JJ, Liddle JA. 2008. Fast, bias-free algorithm for tracking single particles with variable size and shape. *Opt. Express* 16:14064–75
48. Cheezum MK, Walker WF, Guilford WH. 2001. Quantitative comparison of algorithms for tracking single fluorescent particles. *Biophys. J.* 81:2378–88
49. Crocker JC, Grier DG. 1996. Methods of digital video microscopy for colloidal studies. *J. Colloid Interface Sci.* 179:298–310
50. Ma H, Kawai H, Toda E, Zeng S, Huang Z-L. 2013. Localization-based super-resolution microscopy with an sCMOS camera part III: Camera embedded data processing significantly reduces the challenges of massive data handling. *Opt. Lett.* 38:1769–71
51. Wang Y, Quan T, Zeng S, Huang Z-L. 2012. PALMER: a method capable of parallel localization of multiple emitters for high-density localization microscopy. *Opt. Express* 20:16039–49
52. Quan T, Zhu H, Liu X, Liu Y, Ding J, et al. 2011. High-density localization of active molecules using structured sparse model and Bayesian information criterion. *Opt. Express* 19:16963–74
53. Babcock H, Sigal YM, Zhuang X. 2012. A high-density 3D localization algorithm for stochastic optical reconstruction microscopy. *Opt. Nanoscopy* 1:6
54. Mukamel EA, Babcock H, Zhuang X. 2012. Statistical deconvolution for superresolution fluorescence microscopy. *Biophys. J.* 102:2391–400

55. Zhu L, Zhang W, Elnatan D, Huang B. 2012. Faster STORM using compressed sensing. *Nat. Methods* 9:721–23
56. Cox S, Rosten E, Monypenny J, Jovanovic-Talisman T, Burnette DT, et al. 2012. Bayesian localization microscopy reveals nanoscale podosome dynamics. *Nat. Methods* 9:195–200
57. Hu YS, Nan X, Sengupta P, Lippincott-Schwartz J, Cang H. 2013. Accelerating 3B single-molecule super-resolution microscopy with cloud computing. *Nat. Methods* 10:96–97
58. Rosenberg SA, Quinlan ME, Forkey JN, Goldman YE. 2005. Rotational motions of macromolecules by single-molecule fluorescence microscopy. *Acc. Chem. Res.* 38:583–93
59. Backlund MP, Lew MD, Backer AS, Sahl SJ, Grover G, et al. 2012. Simultaneous, accurate measurement of the 3D position and orientation of single molecules. *Proc. Natl. Acad. Sci. USA* 109:19087–92
60. Enderlein J, Toprak E, Selvin PR. 2006. Polarization effect on position accuracy of fluorophore localization. *Opt. Express* 14:8111–20
61. Engelhardt J, Keller J, Hoyer P, Reuss M, Staudt T, Hell SW. 2011. Molecular orientation affects localization accuracy in superresolution far-field fluorescence microscopy. *Nano Lett.* 11:209–13
62. Aguet F, Geissbühler S, Märki I, Lasser T, Unser M. 2009. Super-resolution orientation estimation and localization of fluorescent dipoles using 3-D steerable filters. *Opt. Express* 17:6829–48
63. Pavani SR, Thompson MA, Biteen JS, Lord SJ, Liu N, et al. 2009. Three-dimensional, single-molecule fluorescence imaging beyond the diffraction limit by using a double-helix point spread function. *Proc. Natl. Acad. Sci. USA* 106:2995–99
64. Stallinga S, Rieger B. 2012. Position and orientation estimation of fixed dipole emitters using an effective Hermite point spread function model. *Opt. Express* 20:5896–921
65. Huang B, Jones SA, Brandenburg B, Zhuang X. 2008. Whole-cell 3D STORM reveals interactions between cellular structures with nanometer-scale resolution. *Nat. Methods* 5:1047–52
66. Juette MF, Gould TJ, Lessard MD, Mlodzianoski MJ, Nagpure BS, et al. 2008. Three-dimensional sub–100 nm resolution fluorescence microscopy of thick samples. *Nat. Methods* 5:527–29
67. Mlodzianoski MJ, Juette MF, Beane GL, Bewersdorf J. 2009. Experimental characterization of 3D localization techniques for particle-tracking and super-resolution microscopy. *Opt. Express* 17:8264–77
68. Badieirostami M, Lew MD, Thompson MA, Moerner WE. 2010. Three-dimensional localization precision of the double-helix point spread function versus astigmatism and biplane. *Appl. Phys. Lett.* 97:161103
69. Grover G, Pavani SRP, Piestun R. 2010. Performance limits on three-dimensional particle localization in photon-limited microscopy. *Opt. Lett.* 35:3306–8
70. Sage D, Pengo T, Kirshner H, Stuurman N, Min J, Manley S. 2012. *Localization microscopy: ISBI 2013 challenge*. **http://bigwww.epfl.ch/smlm/challenge2013**
71. Baddeley D, Cannell MB, Soeller C. 2010. Visualization of localization microscopy data. *Microsc. Microanal.* 16:64–72
72. Shroff H, Galbraith CG, Galbraith JA, Betzig E. 2008. Live-cell photoactivated localization microscopy of nanoscale adhesion dynamics. *Nat. Methods* 5:417–23
73. Egner A, Geisler C, von Middendorff C, Bock H, Wenzel D, et al. 2007. Fluorescence nanoscopy in whole cells by asynchronous localization of photoswitching emitters. *Biophys. J.* 93:3285–90
74. Huang Z-L, Zhu H, Long F, Ma H, Qin L, et al. 2011. Localization-based super-resolution microscopy with an sCMOS camera. *Opt. Express* 19:19156–68
75. Saurabh S, Maji S, Bruchez MP. 2012. Evaluation of sCMOS cameras for detection and localization of single Cy5 molecules. *Opt. Express* 20:7338–49